

RSC Advances



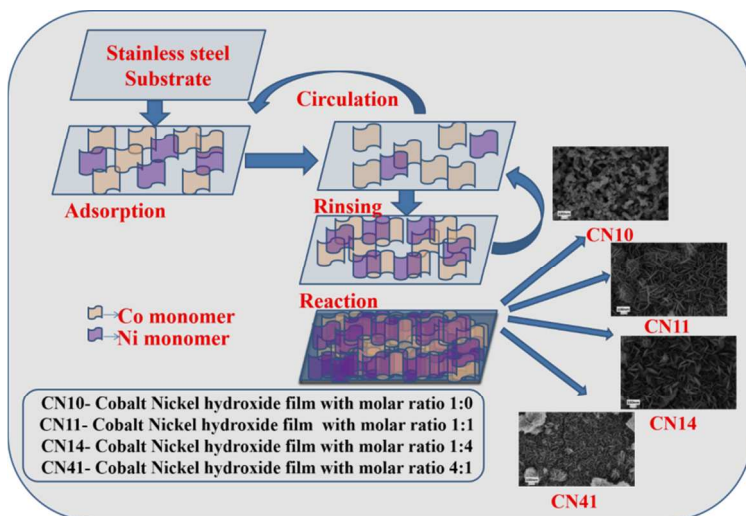
This is an *Accepted Manuscript*, which has been through the Royal Society of Chemistry peer review process and has been accepted for publication.

Accepted Manuscripts are published online shortly after acceptance, before technical editing, formatting and proof reading. Using this free service, authors can make their results available to the community, in citable form, before we publish the edited article. This *Accepted Manuscript* will be replaced by the edited, formatted and paginated article as soon as this is available.

You can find more information about *Accepted Manuscripts* in the [Information for Authors](#).

Please note that technical editing may introduce minor changes to the text and/or graphics, which may alter content. The journal's standard [Terms & Conditions](#) and the [Ethical guidelines](#) still apply. In no event shall the Royal Society of Chemistry be held responsible for any errors or omissions in this *Accepted Manuscript* or any consequences arising from the use of any information it contains.

Graphical Abstract



The schematic of nucleation and growth process during thin film formation of Co/Ni hydroxide films on SS substrate.

Cite this: DOI: 10.1039/c0xx00000x

www.rsc.org/xxxxxx

ARTICLE TYPE

Facile synthesis of amorphous Co/Ni hydroxide hierarchical films and the study of morphology and electrochemical properties

Niraj Kumar^a and H S Panda^{*a}

5 Received (in XXX, XXX) Xth XXXXXXXXXX 20XX, Accepted Xth XXXXXXXXXX 20XX
DOI: 10.1039/b000000x

Amorphous Co/Ni hydroxide films were prepared by using successive ionic adsorption and reaction method (SILAR) on stainless steel substrate and examined their electrochemical properties for supercapacitor application. The amorphous nature of the film was confirmed by powder X-ray diffraction. The vertical align interconnected nano sheet array morphology with uniform distribution was observed from scanning electron microscope and atomic force microscope. Their electrochemical properties were measured by performing cyclic Voltammetry, galvanostatic charge-discharge and electrochemical impedance spectroscopy study in aqueous electrolyte. The specific capacitance was calculated to be 720 Fg⁻¹ at 5mVs⁻¹ for Co/Ni hydroxide, which shows substantial improvement in electrochemical capacitance than the pure cobalt hydroxide. The result suggested the template free deposition method is promising to achieve next generation electrode materials.

15

1. Introduction

Supercapacitors are also called ultra-capacitors or electrochemical capacitors, have obtained great attention in present years due to their high power density, high specific energy, fast recharge capacity, environmental friendly, and outstanding operational life. It can cover the gap between conventional capacitor and batteries [1-3]. At the base of the charge storage mechanism, the supercapacitor is divided into two types: (a) electrical double-layer capacitor (EDLC) and (b) pseudocapacitor. EDLC stores, charge by using electrolyte ion adsorption on the surface of an electrode, and pseudocapacitor stores, charge by fast surface redox reactions [4]. Several types of carbon materials such as activated carbon [5], graphene [6] and carbon nanotube [7] are used in EDLC. However, electrode materials of pseudocapacitor are conducting polymers [8,9], and various oxides/hydroxides of transition metals such as Ru, Co, Ni, Mn etc. [10-13]. Pseudocapacitive electrode materials are furnished higher energy density and specific capacitance than the EDLC electrode materials [14]. Among these pseudocapacitive materials, amorphous hydrated RuO₂ demonstrates prominent properties due to its large specific capacitance (760 Fg⁻¹) and excellent electrochemical stability [15]. But its high cost and toxicity to the environment restricted their commercial applications. Therefore influential efforts have been made to look for an alternative cheap and environmental friendly electrode material with good capacitive behavior for supercapacitor.

Among transition metal hydroxides, Co (OH)₂ and Ni (OH)₂ are used as an appealing electrode material for supercapacitor application due to their high specific capacitance [16,17] (theoretical specific capacitance is around 3460 and 2584 Fg⁻¹ for Co (OH)₂ and Ni (OH)₂ respectively), low cost, and well-defined electrochemical redox activity [18,19]. But the reported specific capacitance is much lower than their theoretical capacitance. Therefore, it encouraged us to synthesize carbon free Bimetal hydroxides of Co and Ni by using a new method for

achieving better electrochemical properties. It is believed that Bimetal hydroxide matrix will increase the electrochemical reversibility, and hence increases the specific capacitance and stability.

Recent years, many synthesis methods such as electro-deposition [20], sputter deposition [21], chemical bath deposition [22], hydrothermal synthesis [23], sol-gel method [24, 25] etc. were adopted to develop various transition metal hydroxides. However, the successive ionic layer adsorption and reaction (SILAR) method has received considerable attention as a soft chemical solution method to deposit a film on various substrates at room temperature. Advantages of SILAR method are robust process, excellent material utilization efficiency, control over film thickness, environmental friendly, flexible and low cost. In this method, films are deposited on a substrate by immersing that in cationic and anionic solution one by one of numerous times to obtain desired thickness. Uniform deposition is possible by this method because the basic building blocks are ions instead of atoms. Recently, Dubal et al. [25] reported the deposition of sponge like β-Ni (OH)₂ on stainless steel substrate by using SILAR method, and the specific capacitance was calculated to be 428 Fg⁻¹ at 5 mVs⁻¹. Further, Kandalkar et al. [26] investigated Co-Ni thin film on copper substrate by applying chemical bath deposition method. They observed irregular shape nano platelet having specific capacitance 324 Fg⁻¹. Chen et al. [27] fabricated three-dimensional macroporous nickel foam and in that cultivated one dimensional Ni-Co layered double hydroxides by using hydrothermal co-deposition method. They used Cetyl trimethyl ammonium bromide as a nanostructure growing template and the specific capacitance was found to be 2682 Fg⁻¹ at 3Ag⁻¹ for asymmetrical supercapacitor. Jökar et al. [28] synthesized Ni-Co binary oxide by using solvo-thermal and the specific capacitance was saturated at 600 Fg⁻¹. Xihong et al. [29] synthesized porous Ni-Co nano sheet array on Fluorine doped Tin Oxide (FTO) substrate by electrochemical method and the specific capacitance was measured to be 453 Fg⁻¹ at 5mVs⁻¹. In summary, several attempts have been made to improve the morphology, film

thickness, porosity and specific capacitance of transition metal oxides/hydroxides. On the other hand, amorphous metal hydroxides offer unique electrochemical behaviours [30, 31]. Li at al. showed improvement in electrochemical efficiency in amorphous $\text{Co}(\text{OH})_2$ due to disordered structure, which is responsible for providing more transportation channels than that of a highly crystalline structure [32]. However, there is no report on amorphous Co/Ni hydroxide film for the application of electrode materials. Further, SILAR method is not implemented so far to prepare Co/Ni hydroxides. This observation prompted us to standardize SILAR method as an alternative process to prepare Co/Ni hydroxide, which would improve the electrochemical properties.

In this work, fast time we prepared amorphous Co/Ni hydroxide films on stainless steel (SS) substrate by using facile and effective SILAR method. The effect of molar ratios of cobalt and nickel on structure, morphology and electrochemical properties was investigated. The amorphous Co/Ni hydroxide film with the uniform and porous morphology was confirmed by scanning electron microscope. The specific capacitance was calculated by performing cyclic Voltammetry and charge-discharge electrochemical study and proved the improvement in capacitive behavior (720 Fg^{-1}) with excellent cyclic stability.

2. Experimental Section

2.1 Synthesis of amorphous Co/Ni hydroxide films and reaction mechanism

Film deposition on a substrate is mainly based on the adsorption and reaction mechanism of the ions from the cationic and anionic solution respectively in two-step SILAR method. The substrate was rinsed in deionized water between every immersion for avoiding the precipitation of loosely bonded materials. The film was grown on the immersed substrate surface due to ion-by-ion deposition at nucleation sites according to the growth kinetics. Rinsing in deionized water enables heterogeneous reaction in solid phase. In a typical process, amorphous Co/Ni hydroxide film was deposited on a stainless steel substrate by SILAR method at room temperature. $5 \times 1 \text{ cm}^2$ stainless steel was used as substrate for depositing the materials.

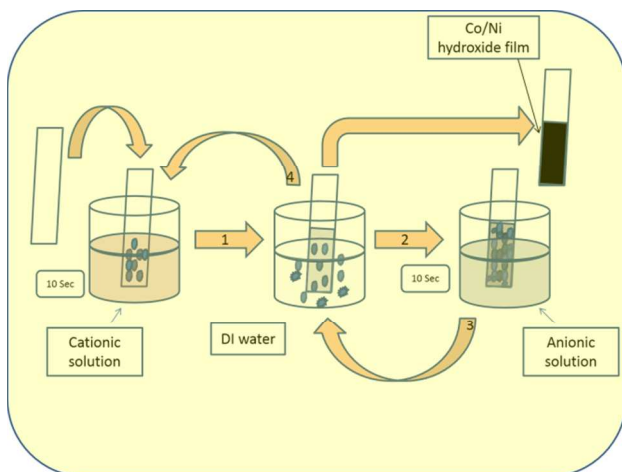
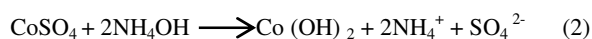
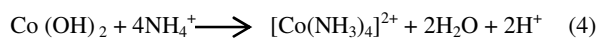
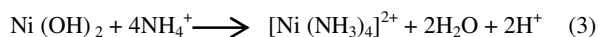


Figure 1. The schematic representation of SILAR method for the synthesis of Co/Ni hydroxide films on the SS substrate.

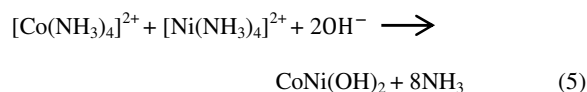
Prior to the deposition, the substrate was washed with deionized water, ethanol and acetone respectively in an ultrasonic bath for 10 minutes. Three beaker systems were used for depositing Co/Ni hydroxide film on a substrate. The first beaker was contained the different molar ratio of $\text{CoSO}_4 \cdot 7\text{H}_2\text{O}$ and anhydrous NiCl_2 as the cobalt and nickel source by maintaining the total molar ratio 0.1. In that, ammonium hydroxide (NH_4OH) was added with constant stirring to adjust the pH (~ 12) for making alkaline solution. When an aqueous ammonia solution was added to the salt solution, the ionic product of nickel and cobalt surpassed the solubility product and the solution turned to turbid due to corresponding hydroxide precipitation according to the following reaction:



Further addition of more ammonium hydroxide reduces the Ni^{2+} and Co^{2+} ion concentration by dissolving the precipitate and forming amminonickel(II) and amminocobalt (II) complex. The mechanism can be expressed by the following reaction:



The substrate was immersed in the above solution for 10 second for absorbing metal complexes onto the substrate due to electrostatic force of attraction between the complex ions and substrate. After that, the substrate was rinsed with deionized water and then placed in the hot water- H_2O_2 solution (90°C) for another 10 second. As a result metal complexes were converted to metal hydroxides, and the mechanism was shown below-



The cycle was repeated for 80 times to attain an optimum thickness. Finally, the film deposited substrate was immersed in deionized water to remove loosely bound ions/particles and dried at room temperature. The process was followed to prepare different molar ratios of cobalt to nickel as 1:0, 1:1, 1:4 and 4:1 and labeled as CN10, CN11, CN14 and CN41 respectively for Co/Ni hydroxide film on SS. Mass loading of the deposited material on the substrate ($5 \times 1 \text{ cm}^2$) is 1.7, 2.0, 2.2 and 1.8 mg for sample CN10, CN11, CN14 and CN41 respectively. The schematic representation of the synthesis and the nucleation and growth process is shown in figure 1 and 2 respectively.

2.2 Characterization

X-ray diffraction (XRD) pattern of the films was obtained by using BRUKER D8 ADVANCE powder X-Ray diffraction having Cu-K α radiation ($\lambda = 1.542 \text{ \AA}$). The morphology of the films was observed by field emission scanning electron microscope (SIGMA, Carl Zesis) and the elemental composition

of the films was analyzed by energy dispersive X-ray analysis (INCA OXFORD). The porosity of the developed films was calculated by using the digital image analysis software. The water contact angle measurements were carried by using a Kruss DSA100 (Germany) contact angle goniometer using deionised water at ambient temperature. Surface roughness of the prepared films were visualized by Asylum Research MPF3D Atomic Force Microscopy (AFM). Cyclic Voltammetry, galvanostatic charge-discharge and electrochemical impedance spectroscopy measurements were performed in an electrochemical workstation (Novocontrol Alpha-A analyzer + POT/GAL). Electrochemical cell consisted of platinum wire as a counter electrode, saturated calomel electrode (SCE) as reference electrode and film deposited stainless steel substrate as working electrode in a three electrode glass cell. $1 \times 1 \text{ cm}^2$ substrates are used for all electrochemical characterization. 1M KOH solution was used as an electrolyte. Cyclic Voltammetry and galvanostatic charge-discharge data were recorded by using WinChem software. The electrochemical impedance spectroscopy (EIS) measurement data was evaluated by WinDeta software in the frequency range 100 KHz to 10^{-1} Hz.

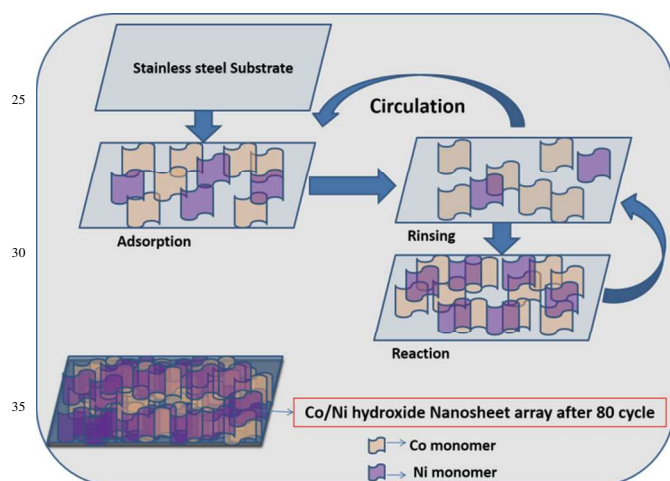


Figure 2. Schematic representation of nucleation and growth process of Co/Ni hydroxide films on SS substrate.

3. Result and Discussion

3.1 Structure and Morphology Study

Figure 3 shows the XRD patterns of blank SS substrate and film deposited SS substrates in the 2θ range $10-80^\circ$. XRD patterns are indexed by using JCPDS software (PDF: 09-0050). Two sharp peaks observed at two theta 43° and 44° due to the SS substrate. There is no additional peaks appeared in the film deposited substrate and confirmed the amorphous nature of the deposited film. The amorphous film is more suited for supercapacitor application owing to more transportation path for ion/electron at the electrode/electrolyte surface [32].

The FESEM micrographs of the developed films are shown in figure 4. Figure 4a shows the spherical morphology of film CN10. The average size of the deposited Co nanoparticles is around 43 nm. However, incorporation of nickel in cobalt

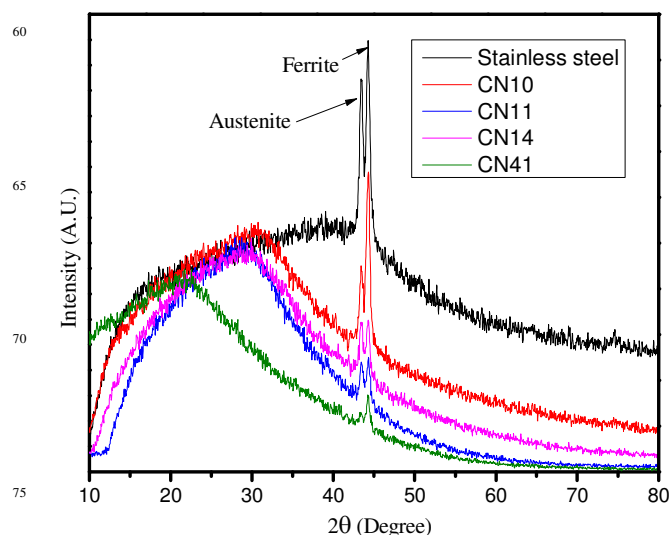


Figure 3. XRD patterns of SS substrate and Co/Ni hydroxide film deposited on SS substrates.

hydroxide and vice versa cause to change the morphology from spherical to vertically align porous interconnected nanosheets arrays. Further, it is clearly evidenced that the size and thickness of nanosheets array changes by changing the molar ratio of the precursor. Percentage of porosity was calculated by using fast and effective total optical porosity method by using Image J software [33, 34]. It was calculated by generating a porosity threshold image and was found to be 27, 62, 63 and 71 for CN10, CN11, CN14 and CN41 respectively. Obtained amorphous hydroxide film (CN41) showed highly hierarchical porous nanosheet array with cavities, which is beneficial to the enhancement of capacitive properties by providing easy charge transport, fast ion/electron transfer, short diffusion path for electrochemical reactions [35]. In cobalt to nickel molar ratio 4:1 (CN41), porous nanosheet distributed evenly and hence improve the electrochemical properties (figure 4d).

Again the impact of porosity on wettability was studied by measuring the contact angle of the developed films. The contact angle was calculated to be 75° , 36° , 32° and 23° for CN10, CN11, CN14 and CN41 film respectively (Fig 4, Insert). The measurement suggested that the wettability was increased by changing the molar ratio of Co and Ni and supported the increase of porosity. This might be due to the increase of surface roughness, porosity and strong polar interaction between water droplets and hydroxide present in the deposited film. Increase [36] in wettability is the desired feature of electrochemical supercapacitor because of the close interaction between electrode/electrolyte interface and also decreases the evolution of oxygen and hydrogen [37].

Figure 5 shows the elemental mapping of thin films, which provided the information about the distribution of the elements. Elements are homogeneously distributed in the deposited amorphous hydroxide films according to the feeding of precursors and also the color of the mapping demonstrates qualitatively the presence of elements in the films.

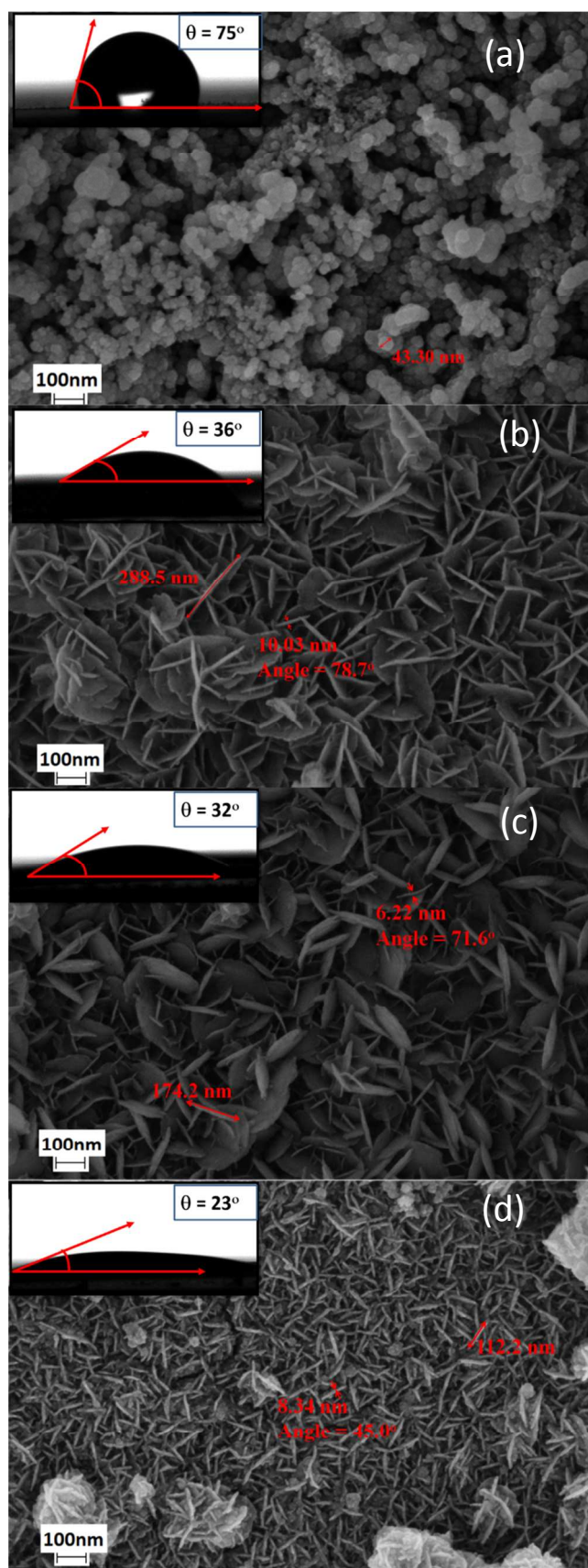


Figure 4. FESEM images of CN10 (a), CN11 (b), CN14 (c) and CN41 (d).

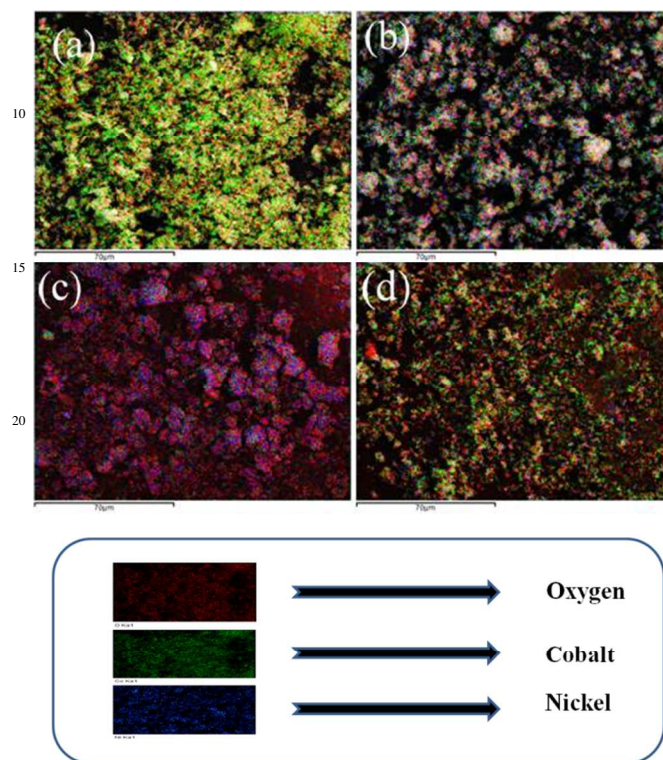


Figure 5. Elemental mapping images of CN10 (a), CN11 (b), CN14 (c) and CN41 (d).

Table 1. Elemental analysis data of the developed hydroxide films

Name of Sample	Element (weight %)		
	Co	Ni	O
CN10	57 ± 0.9	0.00	42 ± 0.1
CN11	27 ± 0.8	17 ± 0.4	54 ± 0.7
CN14	8 ± 0.4	26 ± 0.7	64 ± 0.9
CN41	38 ± 0.5	6 ± 0.2	55 ± 0.3

Further, EDX analysis provides information for the quantitative elemental percentage and estimation of their relative abundance on the surface. It is clearly seen that the oxygen percentage increased significantly with increase in molar ratio of Ni. This is due to (i) the formation of amorphous type NiOOH film [38] and (ii) the larger interlayer space [39] of nickel hydroxides and oxyhydroxides facilitates the adsorption and crystallization of water molecules in the interlayer. Further, increased percentage of oxygen revealed the non-stoichiometry formation of the deposit materials due to their hydrous nature [9]. Table 1 shows the weight percentage of different elements in the developed films.

Figure 6 shows the two dimensional (2D) and three dimensional (3D) images of the films CN14 and CN41 by using Atomic Force Microscope. On the right side of the image, color scale is indicated the height profile of the grains. The color contrast in the image is pointed the surface roughness of deposited films. It is seen from the image that the particles in CN14 (figure 6a) and CN41 (figure 6b) self-assemble as the elevated hill like

distribution and mountain like vertical distribution respectively with the prominent roughness profile. Further, 3D micrograph of the films was suggested the relatively more surface roughness for CN41 than compared to CN14, and resulted the more active sites for electrode/electrolyte interaction.

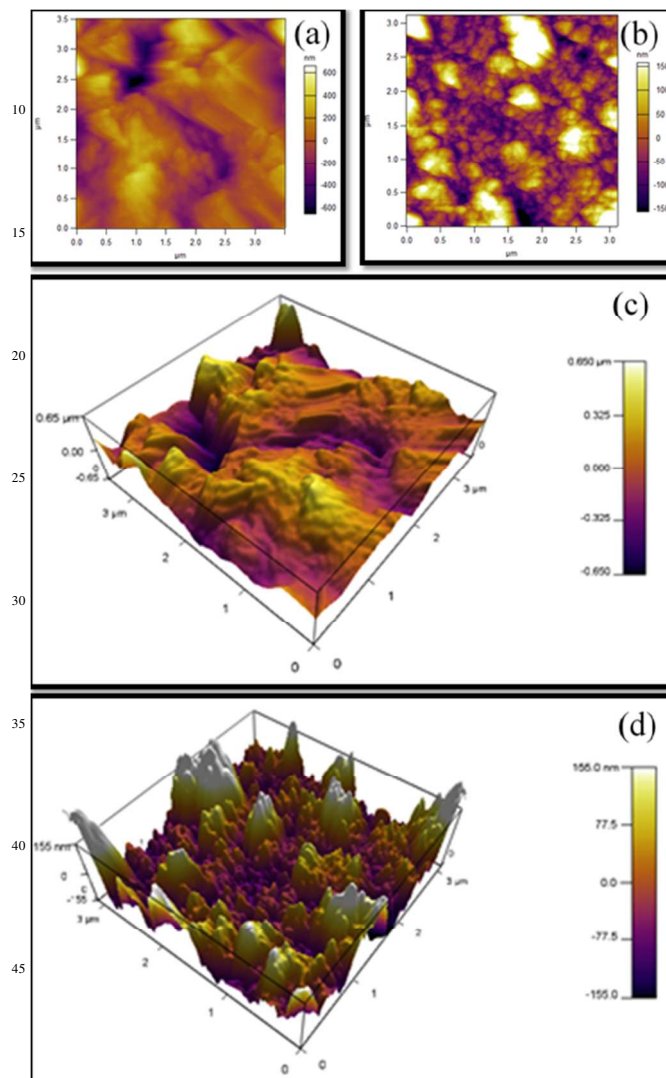


Figure 6. Two dimensional (2D) AFM image of films CN14 (a) and CN41 (b) and three dimensional (3D) AFM image of films CN14 (c) and CN41 (d).

3.2 Electrochemical studies.

All electrochemical studies are accomplished in three electrode system electrochemical cell. In which platinum wire is used as counter electrode and saturated calomel electrode (SCE) is used as a reference electrode in 1 M KOH electrolyte.

Cyclic voltammogram (CV) studies are carried out to study and compare the capacitive behavior of the material deposited on the substrate. Figure 7 shows the CV curves of CN10, CN11, CN14 and CN41 at various scan rates with a potential window of -0.1 to +0.6 V. The shapes of the curves are not rectangular, which indicates that the material behaves strong pseudocapacitive

behavior. The shape of the curve for different molar composite is different due to different nanostructure and morphology, and dissimilar mass loading on the substrate. The films (CN14 and CN41) are shown redox reversible peak and suggested the strong redox behavior of the materials.

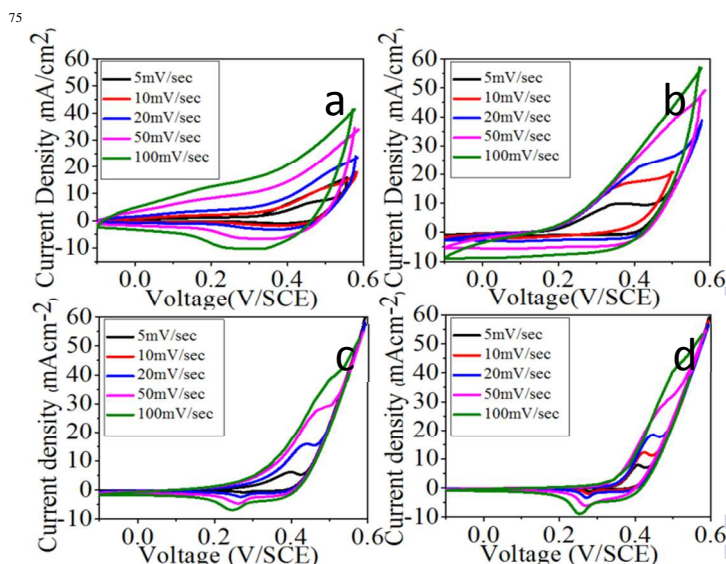
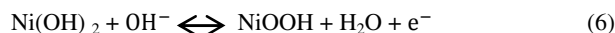


Figure 7. CV curves of CN10 (a), CN11 (b), CN14 (c) and (d) CN41 (d) films at various scan rates.

The redox peak indicated the quasi reversible transfer process as a result of pseudocapacitive capacitance and also showed the symmetrical positive and negative sweep. The anodic peak occurred due to oxidation of Co/Ni hydroxide and the cathodic peak appeared because of reverse process. This process can be expressed by following the reversible equations (6) and (7).



The figure also suggested the effect of increasing scan rate (5 to 100 mVs^{-1}) on the supercapacitive behavior of the amorphous hydroxides. Current under the CV curve slowly increases with increasing the scan rate. The specific capacitance C_s was calculated by using the following relation: [40]

$$C_s = \frac{1}{mv(V_c - V_a)} \int_{V_a}^{V_c} I(V) dV \quad (8)$$

Where m is the deposited mass of the material on the substrate, v is the scan rate, $I(V)$ is the response current, $V_c - V_a$ is the potential window. Integration of response current gives the area of CV curve, which gives the average current. The deposited mass of substrate was calculated by the weight difference method using sensitive microbalance. The electrochemical analysis area of the substrate is $5 \times 1 \text{ cm}^2$ in which the active material deposition is on $1 \times 1 \text{ cm}^2$. The maximum specific capacitance was calculated to be 720 Fg^{-1} for CN41 at a scan rate of 5 mVs^{-1} . This value is higher than the specific capacitance of pristine cobalt hydroxide film CN10 (175 Fg^{-1}) and reported literature for SILAR methods [25]. At the slowest scan rate the obtained specific capacitance gives the closest usage of the electrode materials [41]. At the higher scan rate depletion or saturation of ions increases the ionic

resistivity and decreases the capacitance because of slow transfer of ions in electrode materials. The enhancement of specific capacitance in CN41 film is due to improved morphology, porous architecture, larger surface area, facile transfer path and more active sites for ion diffusion. Figure 8 shows the plot of specific capacitance of the amorphous hydroxide films at different scan rate.

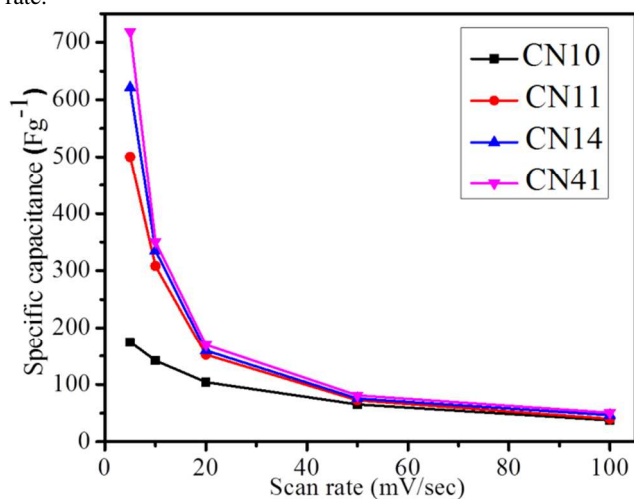


Figure 8. Plot of specific capacitance at various scan rate.

Figure 9 gives the galvanostatic discharge curve of developed electrodes at different current density. The nonlinear and linear shape of the discharge curve indicated the pseudo and double layer capacitance behavior of the electrode materials respectively. The specific capacitance from discharge curve was evaluated by using the following equation [40].

$$C_S = \frac{Q}{\Delta V \times m} = \frac{I \times \Delta t}{\Delta V \times m} \quad (9)$$

Where C_S is the specific capacitance, I is the discharge current, Δt is the discharge time in sec, ΔV is the potential window and m is the mass of deposited material in grams.

The calculated value of the specific capacitance at different current density was shown in Figure 10. The calculated specific capacitance of CN41, CN14 and CN11 is significantly higher than the pristine CN10 sample. Internalization of nickel hydroxide in cobalt hydroxide nanostructure increased the capacitive behavior by improving morphology, surface area, accessibility of electrolyte, contribution of their redox pseudocapacitance, and efficient usage of active sites. The cyclic stability study is an important test to understand electrochemical reversibility and long-term utility of the supercapacitor. Cyclic stability of sample CN14 and CN41 for 2000 cycles at 50 mVs⁻¹ scan rates is shown in figure 11. Sample CN41 is retaining 85% and sample CN14 is retaining 78% of its specific capacitance even after 2000 cycles. Ragone plot is illustrated in figure 11d, which is the plot between energy density and power density. Ragone plot is an efficient way to evaluate the operational performance of the supercapacitor.

Energy density and power density of electrode materials were calculated from the galvanostatic discharge curve by using the following equations [40].

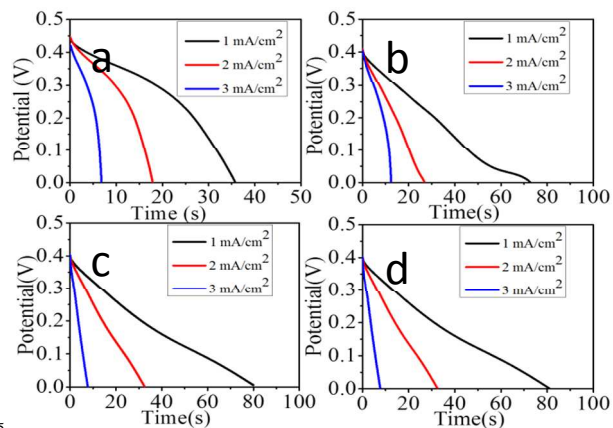


Figure 9. Galvanostatic discharge curves of CN10 (a), CN11 (b), CN14 (c) and CN41 (d) at different current density.

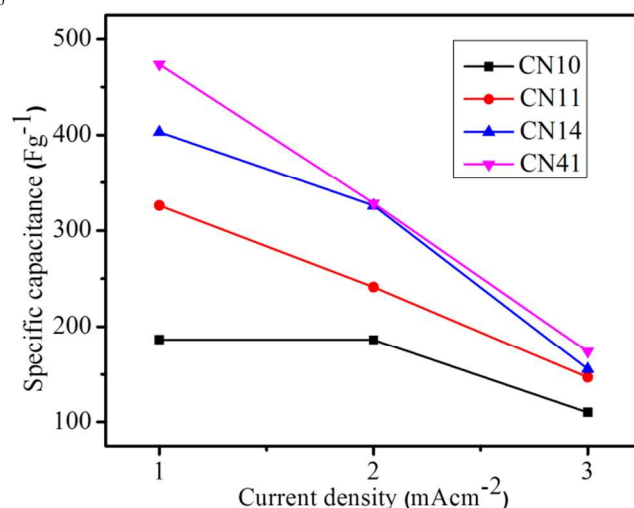


Figure 10. Plot of the specific capacitance of deposited films at different current densities.

$$E = \frac{C_S \times V_{max}^2}{2 \times 3.6} \quad (10)$$

$$P = \frac{E \times 3600}{\Delta t} \quad (11)$$

Where E is the energy density in WhKg⁻¹, P is the power density in WKg⁻¹ and V_{max} is the maximum voltage attained in the discharge process. The graph suggested that the applicability of film CN41 as an electrode material than compared to other developed hydroxide films.

Figure 12 shows a Nyquist plot of the developed electrode materials at the frequency range of 100 KHz to 10⁻¹ Hz with potential amplitude of 0.4 V. The electrochemical impedance spectra (EIS) are helpful to characterize the frequency response on charge transfer process and electrochemical reaction at the electrode/electrolyte interface of active materials. The Nyquist plot consists of real and imaginary parts of the impedance at different frequencies. The high frequency region and fitted equivalent circuit is showed in Fig 12 (Insert). Straight line

perpendicular to the real axis at lower frequency side shows the mass transfer limit and almost semicircle at high frequency factor indicates the faradic charge transfer resistance in Nyquist plot. In the high-frequency region intercept of the semicircle with real axis provides the equivalent series resistance (R_s) and the diameter of the semicircle gives the interfacial charge-transfer resistance (R_{ct}). R_s comes from solution resistance as well as contact resistance and R_{ct} is due to interfacial charge transfer

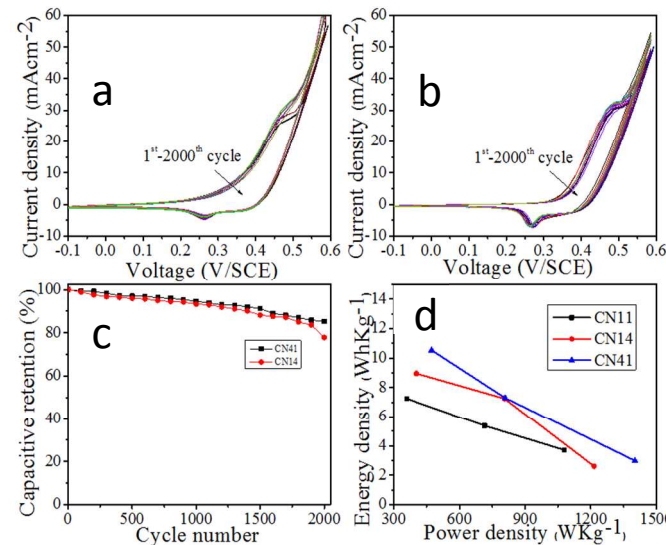


Figure 11. CV curves plot for stability test of CN14 (a) and CN41 (b) deposited films up to 2000 cycles; capacitive retention plot of deposited films (c); Ragone plot of films CN11, CN14 and CN41 (d).

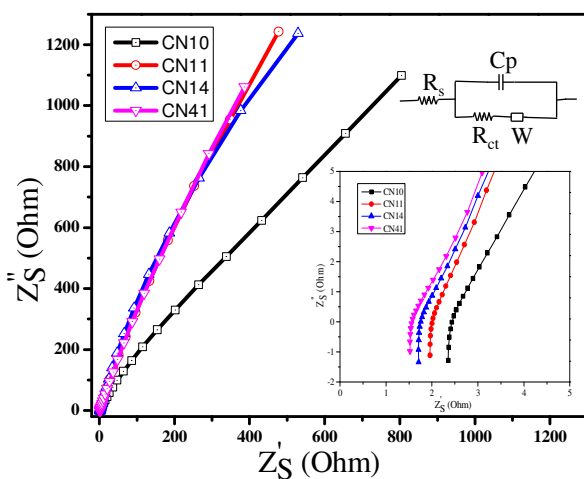


Figure 12. The Nyquist plots of deposited films.

resistance between electrode and electrolyte. C_p in the equivalent circuit represents the pseudocapacitance and W is the Warburg impedance [42]. The slope of the straight line in low frequency is Warburg impedance, which is an effect of ion diffusion resistance between electrode and electrolyte. Increase in slope indicates the better capacitive behavior due to decrease in diffusion resistance and ion diffusion length of the electrode/ electrolyte [43]. Table 2 shows the measured and calculated electrochemical resistance

parameters R_s and R_{ct} for developed amorphous films. The slope of the Nyquist

Table 2. Calculated electrochemical resistance of deposited films

Sample Name	Electrochemical Resistance Parameter	
	R_s (Ωcm^{-2})	R_{ct} (Ωcm^{-2})
CN10	2.354	2.452
CN11	1.958	2.030
CN14	1.711	1.775
CN41	1.521	1.542

plot was suggested that the composite hydroxide films are showing improved capacitive behaviour than the pure cobalt hydroxide (CN10) film. EIS study supported further the more prominent capacitive behaviour and better transportation of charge between electrode/electrolyte of CN41 than the other developed films.

4. Conclusions

In this study, we were synthesized successfully the amorphous Co/Ni hydroxide film by using facile, green and cost efficient binder less SILAR method. It was confirmed that the incorporation of nickel in cobalt hydroxide enhances the electrochemical properties due to the improve redox reversibility and porous morphology. Highest specific capacitance (720 F/g at 5 mVs^{-1}) with add to cyclic stability was achieved fast time when Co to Ni molar ratio 4:1. Vertically aligned porous morphology array was obtained by incorporating Ni in cobalt hydroxide and suggested a better electrode material for supercapacitor.

Acknowledgements

The authors acknowledge the Department of Science and Technology (DST), Govt. of India for financial support.

Notes and references

- ^a Department of Materials Engineering, Defence Institute of Advanced Technology, Girinagar, Pune-411025, India. Fax: XX XXXX XXXX; Tel: 91-20-24304205; E-mail: himanshusp@diat.ac.in
- B E. Conway, Transition from "supercapacitor" to "battery" behaviour in electrochemical energy storage. *J Electrochem Soc* 1991, 138, 1539–1548.
 - P. Simon, Y. Gogotsi, *Nat Mater* 2008, 7, 845–854.
 - J R Miller, P Simon, *Electrochemical capacitors for energy management. Science* 2008, 321, 651–652.
 - B.E. Conway, W.G. Pell, *J. Solid State Electrochem* 2003, 7, 637–644.
 - Qing Zhang, Jiepeng Rong, Dongsheng Ma, Bingqing Wei, *Energy Environ. Sci.* 2011, 4, 2152–2159.
 - Hui Pan, Jianyi Li, Yuan Ping Feng, *Nanoscale Res Lett.* 2010, 5, 654–668.
 - Dingshan Yu, Liming Dai, *J. Phys. Chem. Lett.* 2010, 1, 467–470.
 - Ki-Seok Kim, Soo-Jin Park, *J Solid State Electrochem* 2012, 16, 2751–2758.
 - D.P. Dubal, S.V. Patil, W.B. Kim, C.D. Lokhande, *Materials Letters* 2011, 65, 2628–2631.

- 10 P. R. Deshmukh, S. N. Pusawale, A. D. Jagadale, C. D. Lokhande, *J Mater Sci* 2012, 47, 1546–1553.
- 11 S. Vijayanand, R. Kannan, H. S. Potdar, V. K. Pillai, P. A. Joy, *J Appl Electrochem* 2013, 43, 995–1003.
- 5 12 Liangyu Gong, Xiaohong Liu, Linghao Su *J Inorg Organomet Polym* 2011, 21, 866–870.
- 13 Yong Zhanga, Guang-yin Li, Yan Lv, Li-zhen Wang, Ai-qin Zhanga, Yan-hua Song, Bei-li Huang, *international journal of hydrogen energy* 2011, 36, 11760-11766.
- 10 14 Simon P. Gogotsi Y. Materials for electrochemical capacitors. *Nat Mater*, 2008, 7, 845–854.
- 15 15 Chi-Chang Hu, Kuo-Hsin Chang, Ming-Champ Lin, Yung-Tai Wu, *Nano letters* 2006, 6, 2690-2695.
- 16 Y. Wang, Z. Zhong, Y. Chen, C.T. Ng, J. Lin, *Nano Res.* 2011, 4, 695–704.
- 17 L. Cao, F. Xu, Y. Liang, H.L. Li, *Adv. Mater.* 2004, 16, 1853– 1857.
- 18 X. Zhang, W. Shi, J.Zhu, W. Zhao, J. Ma, S. Mhaisalkar, T.L. Maria, Y. Yang, H. Zhang, H. H. Hng, *Nano Res.* 2010, 3, 643–652.
- 20 19 J. Jiang, J. Liu, R. Ding, J. Zhu, Y. Li, A. Hu, X. Li, X. Huang, *applied materials & interfaces* 2011, 3, 99-103.
- 20 Aghazadeh, Mustafa, *J Appl Electrochem* 2012, 42, 89–94.
- 21 J. H. Lim, D. J. Choi, W. I. Cho, Y.S. Yoon, *J Korcan Phys Soc* 2001, 39, S382.
- 25 22 X. H. Xia, J. P. Tu, X. L. Wang, C. D. Gu, X. B. Zhao *J. Mater Chem* 2011, 21, 671.
- 23 Z. Yongqi, X. Xinhui, K. Jing, T. U. Jiangping, *Chin Sci Bull* 2012, 57, 32.
- 30 24 J. Cheng, G. Cao, Y. Yang, *Journal of Power Sources* 2006, 159, 734-741.
- 25 L. Mai, F Yang, Y. Zhao, X. Xu, L Xu, Y. Luo, *Nature communications*, 2011, 2, 381.
- 35 26 P. Dubal, S. H. Lee, W. B. Kim, *Mater Sci* 2012, 47, 3817–3821.
- 27 S. G. Kandalkar, H. Lee, S. H. Seo, K. Lee, C. Kim, *J Mater Sci* 2011, 46, 2977–2981.
- 28 E. Jokar, A. I. zad, S Shahrokhian, *J Solid State Electrochem*, 2014, 10.1007/s10008-014-2592-y.
- 40 29 X. Lu, X. Huang, S. Xai, T. Zhai, C. Wang, P. Zhang, M. Yu, W. Li, C. Liang, Y. Tong, *J. Mater. Chem.* 2012, 22, 13357.
- 30 H. B. Li, M. H. Yu, F. X. Wang, P. Liu, Y. Liang, J. Xiao, C. X. Wang, Y. X. Tong, G. W. Yang, *nature communications*, 2013, 4,1-7.
- 45 31 H. B. Li, M. H. Yu, X. H. Lu, P. Liu, Y. Liang, J. Xiao, Y. X. Tong, G. W. Yang, *ACS Appl. Mater. Interfaces*, 2014, 6, 745–749.
- 32 V.D. Patake, S.S. Joshi, C.D. Lokhande, Oh-Shim Joo, *Materials Chemistry and Physics*, 2009,114, 6–9.
- 50 33 C. Grove,D.A. Jerram, *Computers & Geosciences* 2011, 37, 1850-1859.
- 34 A. Hadjizadeh, A. Ajji, M. N. *Journal of the mechanical behavior of biomedical materials*, 4, 340–51 (2011).
- 35 D. Feng, Y. Lv, Z. Wu, Y. Dou, L. Han, Z. Sun, Y. Xia, G. Zheng, D. Zhao, *J. Am. Chem. Soc.*, 2011, 133, 15148–15156
- 55 36 J. Shang,M. Flury, J.B. Harsh, R.L. Zollars, *Colloid Interface Sci.* 2008, 328, 299–307.
- 37 B.T. Shivanand,M. Serena, S. Arcadio, G.C. Eloya, A.D. Javier, *Ind. Eng. Chem. Res.*, 2013, 52, 9470–9479.
- 60 38 A. Vander Ven, D. Morgan, Y. S. Meng, G. Ceder, *Journal of The Electrochemical Society*, 2006, 153, A210-A215.
- 39 P. Oliva, J. Leonardi, J. F. Laurent, C. Delmas, J. J. Braconnier, M. Figlanz, F.Fieviet, A. De Guibert, *J. Power Sources*, 1982, 8, 229.
- 65 40 G.S. Gund, D.P. Dubal, S. S. Shinde, C.D. Lokhande *ACS Appl Mater Interfaces* 2014, 6, 3176.
- 41 T. P.Gujjar, W.Y.Kim, I Puspitasari, K. D. Jung, O. S. Joo *Int J Electrochem Sci* 2007, 2,666.
- 42 M. S. Wu, H. H. Hsieh, *Electrochim. Acta*, 2008, 53, 3427-3435.
- 70
- 43 S Vijayakumar, S Nagamuthu, G. Muralidharan, *Appl Mater Interfaces*, 2013, 6, 2188-96.